DEVELOPMENT OF SHINGLE MATRIX TECHNOLOGY FOR INTEGRATED PV APPLICATIONS

[1]Daniel von Kutzleben, [1]Torsten Rößler, [1]Max Mittag [1]Julian Weber, [1]Sanjeev Sigdel, [1]Nils Klasen, [2]Philipp Zahn, [1]Achim Kraft, [1]Holger Neuhaus
[1]Fraunhofer Institute for Solar Energy Systems ISE, Freiburg, Germany
[2]M10 Solar Equipment GmbH, Freiburg, Germany

ABSTRACT: Linear shingling of solar cells has already been known for many years. This work evaluates a new approach of arranging the shingle cells, called matrix shingling and discusses advantages and challenges of this technology. An overview of the most crucial process steps to build matrix modules is presented. Cell-to-module (CTM) simulations are used for a profound loss/gain analysis from host cell to module. A comparison between half-cell modules and matrix modules shows the potential of the matrix technology. Glass facade elements for building integrated PV with red MorphoColor® coating are demonstrated to show the potential of this growing field of application.
Keywords: photovoltaic module, shingling, ECA, BIPV, CTM

1 INTRODUCTION

The most recent part of the IPCC report [1] stated that the most effective way to avoid greenhouse gas emissions is the deployment of wind and solar energy, since it results in the lowest cost per ton of CO_2 saved. Large-scale PV installations require immense areas of land that compete with other uses such as agriculture, forestry, or built-up areas. Therefore, multiple uses of space are necessary. Building integrated photovoltaics (BIPV) is one of those solutions. Architects and building owners, however, are keen not to make their building look like a power plant but to use the solar modules as a design and creative element.

For the growing market of integrated photovoltaics, modules with high requirements to the aesthetic appearance are demanded. Yet, an appealing cell interconnection technology is missing. As shingle interconnection of solar cells enables highly uniform PV modules it particularly fulfills these aesthetical demands. Shingling is known for a long time as interconnection method for solar cells [2]. Companies like Sunpower/Maxeon, Solaria and Tongwei have offered shingled solar modules as commercial products for many years [3–5]. Several manufacturers have placed patents, protecting their intellectual property on some aspects along the production chain. The general idea of shingling solar cells is used since the 1960s and cannot be part of any patent leaving the possibility open for new “players” to enter the BIPV market.

In this scientific work an advanced concept of shingling solar cells is discussed that is called shingle matrix technology [6]. Shingling in the matrix arrangement was already introduced in 1990 [7]. This approach not only contains the advantages of linear shingling but further increases active area in the module and brings a high shading resilience for an increased energy harvest in partial shading situations, which occur more likely in integrated PV [8, 9]. Figure 1 shows a matrix module with red MorphoColor® [10, 11] used to demonstrate colored facade elements.

Section 2 gives an overview about the principle of shingle matrix interconnection, the laser separation process and the shingle matrix stringer followed by a simulated comparison between a half-cell module design and matrix modules. In section 3, produced shingle matrix modules are presented and analyzed in terms of their cell-to-module losses and gains.

Figure 1: Full-size glass-glass matrix module with red MorphoColor® coating as a glass facade element suitable for building integration. The upper left corner is without MorphoColor® to show the matrix cell arrangement.

2 SHINGLE MATRIX TECHNOLOGY

2.1. Shingle matrix interconnection

The matrix technology is an innovative and challenging approach to further improve shingling technology. Although small-scale, lab-type “matrix shingle” modules were shown in the past [7], only Fraunhofer ISE and M10 Solar Equipment have upscaled the shingle matrix technology to improve aesthetics, efficiency [12] and circumvent patent blockades of the conventional shingle interconnection. As a result of this project an industrial stringer machine is ready to bring this innovative approach to the PV market [13]. Fraunhofer

ISE sees a high demand for PV modules that visually satisfy the highest expectations for the market of integrated PV.

The concept of matrix shingling is based on the principle of linear shingling, depicted in Figure 2, but includes an additional lateral offset in every second row by inserting half shingles in the outermost columns.

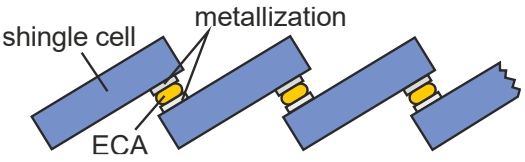

Figure 2: Principle of shingling solar cells. The cells overlap with their busbar metallization and are mechanically and electrically bonded by an electrically conductive adhesive (ECA).

It is the same principle as of a masonry wall. The result is a matrix of flexible length and width, where the shingle cells of one row are connected in parallel by using the busbars of the cells overlapping this row. The rows are in series connection with each other. A drawing of a matrix can be seen in Figure 3. High flexibility in length and width of the shingle matrix is one of its core advantages especially interesting for building integrated applications with predefined glass sizes.

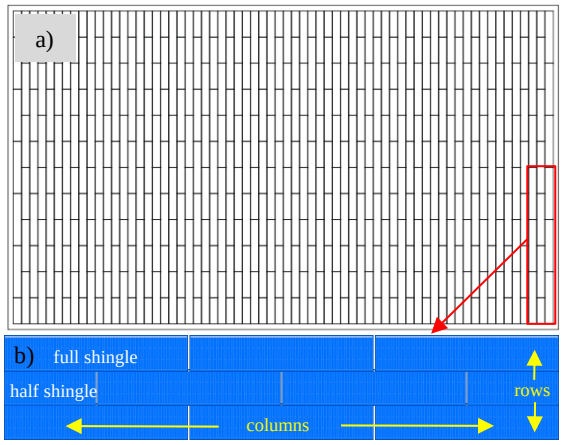

Figure 3: Drawing of a) a full-size matrix module and b) part of the matrix with three full shingle cells in parallel and three rows in series interconnection.

Matrix shingling offers the same advantages as linear shingling, namely lead-free cell interconnection, high active module area and a homogeneous appearance resulting from the absence of ribbons and not existing or minimized cell gaps, respectively. The biggest advantage over linear shingling, however, is the high shading resilience [8, 9]. Partial shading is an issue that must be considered, especially in the field of integrated PV. Matrix modules with a significantly higher power output in situations of shading caused by traffic signs, bird droppings or leaves are predestined for this application. In the case of a matrix module, shaded cells can be circumvented by the current using the lateral current paths through the busbars of adjacent solar cells [14]. In case of diagonal shading, a matrix module can reach up to 73.8% and in the case of random shading 96.5% more power output compared to a module with linear shingle strings [8, 9]. The implementation of the shingle matrix technology comes along with significant technology challenges such as parallel processing of shingles, terminal and intermediate connections and handling of the matrix.

2.2. Laser separation processes

To obtain shingle cells, host wafers must be cut into $1/5^{th}$ to $1/7^{th}$ stripes of the original cell. A common way to separate shingle host cells into shingle cells is by means of a laser. There are two industrially relevant laser cutting processes: Laser scribing and mechanical cleaving (LSMC) [12, 15] and thermal laser separation (TLS) [12, 16]. Both separation processes result in unwanted recombination of charge carriers at the cut edges. However, LSMC is known to lead to larger recombination related efficiency losses compared to TLS when separating the intact host wafer. In Figure 4 is an overview of efficiency of the initial host wafer and cut shingles. The shingles are $1/5^{th}$ of a G1 PERC host cell with the size of 158.75 × 31.75 mm^2. The datapoints of the host wafer are divided by five to make the comparison more comprehensible. The shingles are subdivided into pseudo-square (PSQ) and full-square (FSQ) for LSMC and TLS. PSQ shingles are the two outer shingles of a host cell with only one laser separated edge while the FSQ have two.

The host wafers have a power of 5.5 W_p measured with GridTouch (1.1 Wp if, naively, divided by 5). FSQ/LSMC shingles show a power of 1.04 W_p, while FSQ/TLS shingles feature 1.06 W_p. The corresponding PSQ cells show slightly higher efficiency. The shingles are measured with pin bars between front- and rear side busbar [12]. The difference between host cell and shingle can be separated into two effects. One is a higher series resistance due to increased finger length resulting from the different measurement methods between host cell and shingle, explained in [17]. The second effect is edge recombination on the unpassivated lasered edges. In case of a full-size matrix module with a number of 324 cells, the difference in power output between LSMC FSQ and TLS FSQ cells would be 6.5 W_p. Passivated edge technology (PET) developed by Fraunhofer ISE can recover up to $0.1\%_{abs}$–$0.4\%_{abs}$ of the efficiency losses due to recombination for PERC solar cells [18].

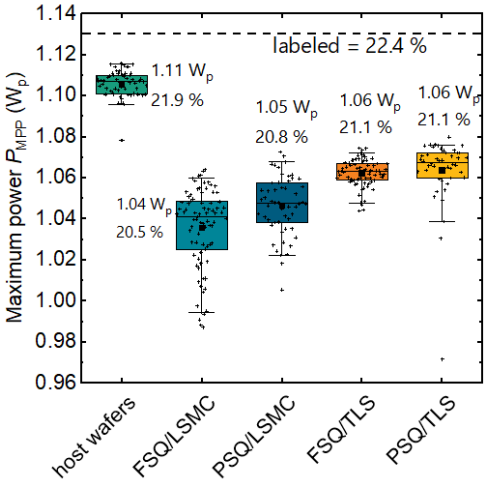

Figure 4: Effect of laser separation processes on the maximum power P_{MPP} of a shingle. LSMC cut shingle

cells show slightly higher cell division losses than TLS cut shingles. For better comparison the host wafer power is divided by 5.

2.3. Shingle matrix stringer

For the matrix modules produced in this work cell arrangement and interconnection are performed on a shingle matrix stringer built by M10 Solar Equipment (Figure 5). Cut shingle cells are used as input material. Controlled by a vision system, the cells are placed row wise in the matrix configuration. Dispensing units are used to apply electrically conductive adhesive (ECA) on the rear side busbar of each shingle after which the rows are placed with the specified offset on an assembling tray. A curing unit using infrared lamps follows. The matrix is transferred by a full-size vacuum gripper and placed on a glass-ethylene-vinyl acetate (EVA) stack. In the last step before the lamination process, terminal and intermediate connectors are attached and prepared for connection with the junction boxes, followed by an EVA and backsheet layer. The stringer is flexible in width and length of the matrices to be produced. This opens up design possibilities for BIPV applications.

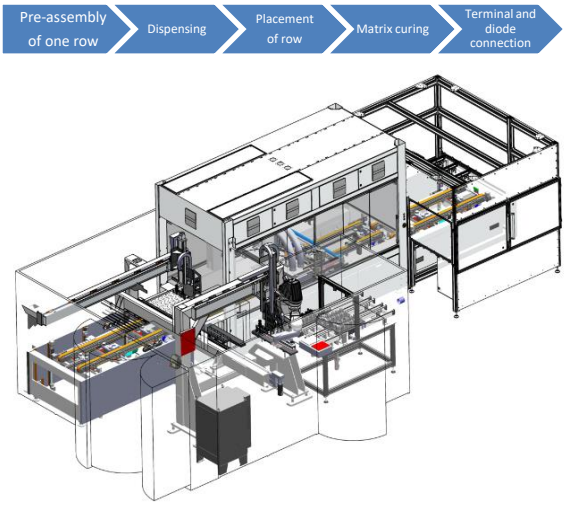

Figure 5: Prototype Shingle Matrix Stringer developed in the project SHIRKAN by M10 Solar Equipment.

Table 1: Comparison of two scenarios for an optimized matrix module with a half-cell module (drawings not to scale).

			Scenario 1	Scenario 2
	Unit	Half-cell	Same host wafer	Same module area
Dimensions	mm^2	1680.5 ×1002.5	1601.5 × 995.0	1693.0 × 995.0
Cell spacing/overlap	mm	1	−1	−1
String spacing/lateral offset	mm	2.0	0.5	0.5
Edge spacing	mm	17	17	17
Top/bottom spacing	mm	34.5	28	28
Center spacing	mm	12.5	-	-
Interconnection	-	5 busbars	ECA	ECA
Module area	m^2	1.685	1.592	1.685
Number of host wafers	-	60	60	63.6
Separated cell efficiency	%	21.6	21.1	21.1
Input power cell level	W_p	326	319	338
Module efficiency	%	18.6	19.2	19.3
Module power	W_p	313	306	324

2.4. Host-cell-to-module prediction

If the shingle matrix technology wants to take a foothold on the market, it must be able to compete with the established half-cell module designs. To find out if and under which conditions matrix technology has advantages in terms of electrical performance, a comparison between a standard half-cell module and two different scenarios for the shingled matrix technology is made by means of cell-to-module (CTM) SmartCalc.Module simulations. Table 1 gives a comprehensive overview about the input and output data for the simulation. The first scenario is using the same number of G1 host wafers as in the half-cell module, namely 60. If those host wafers are cut into shingle cells and interconnected with an overlap the module area is smaller than the one of the half-cell module. The second scenario shows the case of the same module area as the half-cell module by using more host wafers in the shingle module. Starting point for the simulation is the shingle host wafer efficiency of 21.9% corresponding to a maximum power of 1.11 W_p (5.55 W_p for the full wafer) in Figure 4. In case of the shingle module simulations, shingle cells with an efficiency of 21.1% corresponding to the FSQ/TLS cut shingles with a power of 1.06 W_p taken from Figure 4 are used as input for the SmartCalc.Module calculations [19, 20]. To estimate the half-cell efficiency starting with the same 21.9% host wafer efficiency a reduction of $-0.2\%_{abs}$ to consider cutting losses was found to be reasonable [21]. The increased finger resistance of a pin-based measurement in comparison to the GridTouch measured cell was considered to lead to a $-0.1\%_{abs}$ loss [17]. The half-cell input efficiency for the SmartCalc.Module simulation was therefore 21.6%, corresponding to 326 W_p of cell power. The module output is 313 W_p with an efficiency of 18.6% on an area of 1.685 m^2.

Scenario 1: If the same host wafer equivalent number of cells is interconnected in matrix configuration the module area can be reduced to 1.592 m² to avoid unreasonably high unused space. The output power is 7 W_p lower than the power of the half-cell module due to the cell overlap of 1 mm as well as the missing cell and string distances. However, efficiency is enhanced by 0.6%$_{abs}$ to 19.2% because of higher packing density.

Scenario 2: The module area is kept constant in comparison to the half-cell module and thus the number of host wafers is increased to 63.6 (additional 18 shingle cells). The input power on cell level is therefore 12 W_p higher, 338 W_p in total. The module ends up with an efficiency of 19.3% and a power of 324 W_p. This leads to an increase in efficiency of 0.7%$_{abs}$ compared to the half-cell module and to an 11 W_p higher power output on the same module area.

This study shows mainly two things. First, either module area or number of host cells have to be adapted going from half-cell to shingle module. Second, shingling does not necessarily achieve high CTM_{power} ratios (the shading in the overlap is typically a significant power loss factor). However, shingling reaches large power densities: Power output considering a certain module area, which means it delivers higher module efficiencies.

In case of half-cell module technology, the drop in efficiency from the GridTouch measured host wafer to five busbar interconnected half-cell is relatively low (finger resistance and edge recombination) while it is high from half-cell to module (cell and string spacing, loss in the ribbons). In shingling it is rather opposite with a high efficiency loss from host wafer to shingle cell (finger resistance and edge recombination) and a moderate drop from shingle cell to module (no or almost no cell and string spacing, no ribbons). To improve the efficiency of matrix shingle technology we see the introduction of edge passivation as an important next step.

3 EXPERIMENTS AND RESULTS

3.1. Full size modules

Seven full format shingle matrix modules made from industrial G1 PERC shingle cells are manufactured, one of those modules is depicted in Figure 6. Two different ECAs are used. The modules were laminated as glass-backsheet stack in an industrial laminator from Bürkle. The encapsulation materials are EVA and a black polyethylene terephthalate (PET) backsheet. An antireflection coated solar glass with the dimensions of 1700 × 1000 × 3.2 mm^3 is used. The reached power and efficiency for all modules is depicted in Figure 7. The power ranges between 316 W_p and 322 W_p. The best module shows a shingle-to-module power loss of −4.5% with a cell power of 337 W_p and a module power of 322 W_p. Efficiency changes from 20.5% at cell level to 18.8% at module level. A gain and loss analysis for the manufactured modules follows in the next chapter.

3.2. Shingle module CTM analysis

For the full-size matrix modules with the size of 1708 × 1006 mm^2 (glass and frame) having 6 columns and 54 full-shingle-equivalent rows, power and efficiency gains and losses are analyzed. Due to practical reasons, changes in the module design are made in comparison to the presented optimized matrix modules from section 2.4. The main differences are bigger glass margins due to available glass sizes and the usage of one inactive shingle cell row which is used to implement the end contact. Although TLS cut shingle cells potentially lead to higher module efficiency, LSMC cut shingles are used since an automated TLS process was not accessible by the time of module manufacturing. The shingle overlap is increased to 1.3 mm to meet the metallization design of the used shingle solar cells. Theoretical module efficiency (19.3%, from Table 1) and experimental results (18.8%, from Figure 7) show therefore a deviation of 0.5%$_{abs}$. In the next paragraph the power and efficiency loss from shingle cell to module using real data from the built modules are explained.

Figure 6: Full size matrix module with the dimensions of 1708 × 1006 mm^2 manufactured on the Shingle Matrix Stringer. The module features a power of 322 W_p and an efficiency of 18.8%.

Table 2 gives an overview on the *I-V* performance beginning with the host wafer values measured with GridTouch at Fraunhofer ISE. Industrial shingle host cells are labeled with a certain power by the manufacturer, but it stays unclear which measurement setup was used. Therefore, the datasheet values can drastically differ from measurements conducted at Fraunhofer ISE. A GridTouch measurement of host wafers can be a practical workaround, but highly overestimates the performance of separated shingles. The separated shingle cells, measured by pin arrays on the front side and rear side busbar lead to a more realistic value since the current paths are the same as in the interconnected state as well as the effect of edge

recombination losses are included in the measurement. A thorough study about this topic can be found in [17]. According to Table 2 the pin array measured LSMC/FSQ shingles have an efficiency of 20.5%, which is 1.4% $_{abs}$ lower than the host cell efficiency. The values measured for separated shingles are used to analyze the shingle-to-module losses of the built modules with a SmartCalc.Module calculation. The detailed gains and losses in power and efficiency are shown in Figure 8.

The biggest drop in efficiency results from very high glass margins (k1, −1.8%). Interconnection shading (k7) of blue cell area inside the overlap leads to a power loss of 9.5 W_p and an efficiency loss of 0.55%$_{abs}$, respectively. The loss due to the resistance induced by interconnection (k12) is calculated based on assuming a specific contact resistance between ECA and busbars of 0.2 mΩcm^2. This value is within the range given in [22] and based on current investigations at Fraunhofer ISE. As a result, the ohmic power loss proposed by the Smartcalc.Module simulation is 2.5 W_p and −0.1%$_{abs}$ efficiency loss. Note that the factors k1 to k15 that yield a large power loss at the same time correspond to the greatest potential to improve module efficiency.

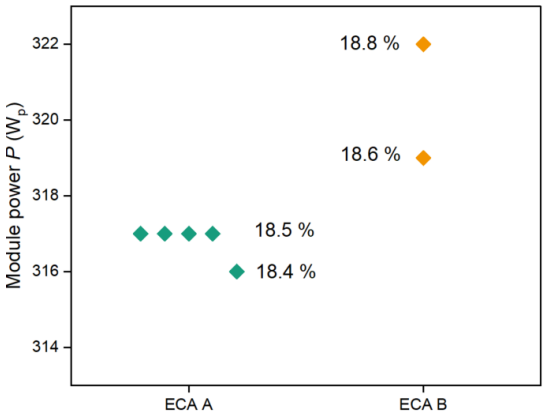

Figure 7: Module power and efficiency of full format matrix modules with two different ECAs.

Table 2: Overview of measured values from host cell to module for fill factor (*FF*), maximum power (P_{MPP}) and efficiency (η).

Description	***FF* (%)**	**P_{MPP} (W_p)**	**η (%)**
Host cell based on Fraunhofer ISE GridTouch measurement	80.8	5.55	21.9
Shingle measured with pin arrays	76.9	1.04	20.5
Produced module (non-optimized) (1.718 m^2)	76.3	322	18.8
Optimized module (SmartCalc.Module simulation) (1.685 m^2)	See scenario 2 in Table 1		

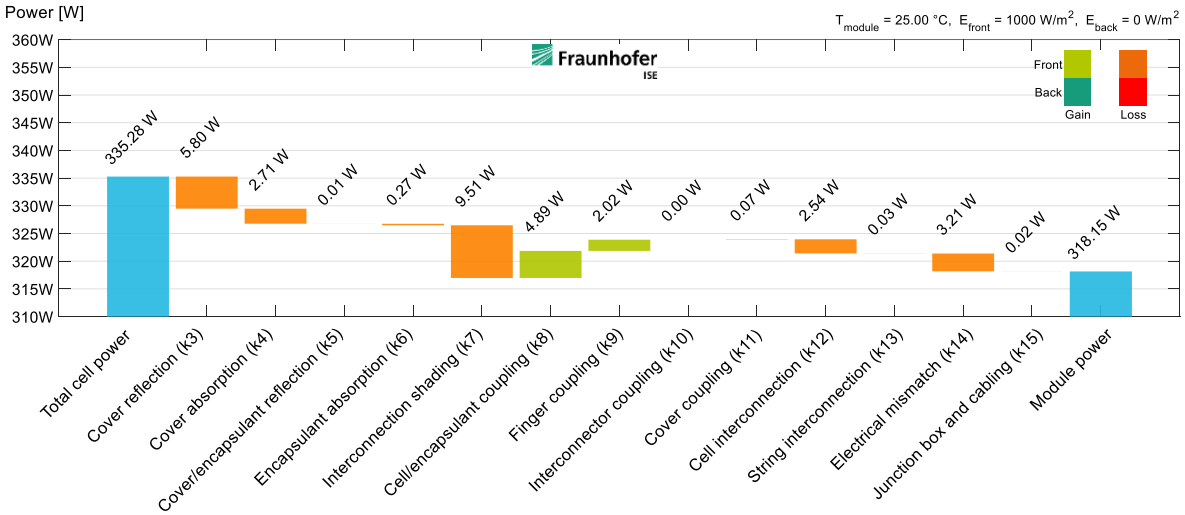

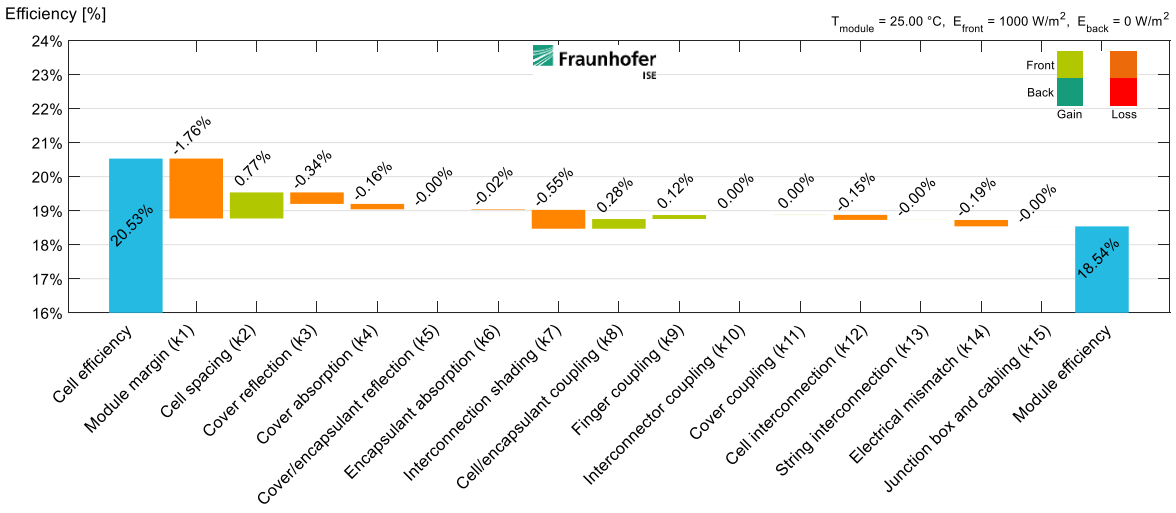

Figure 8: Shingle to module gains and losses diagram for a full-size shingle matrix module as depicted in Figure 6 with G1 1/5th LSMC cut FSQ shingles as input. The factors relevant to the matrix technology are discussed in section 3.2. A detailed description of all factors can be found in [20].

4 CONCLUSION AND OUTLOOK

In this work matrix shingling was analyzed. This technology brings many advantages for BIPV, but for standard modules as well. The absence of ribbons and the bricked wall like arrangement ensure a very homogeneous appearance. High power outputs during partial shading compared to conventional modules ensure high energy yields. Scalability makes integration into predefined glass sizes easy and maintains excellent area efficiency. Better coverage of the module area with cells leads to higher module efficiency. Fraunhofer ISE has developed and tested this technology while an industrial stringer was brought to the market by M10 Solar Equipment. The key points for designing of high efficiency matrix modules are a low damage laser cutting process, optimized glass margins and reduced shingle overlap. A comparison between a common half-cell module and matrix modules shows that either module area or number of host cells must be adjusted for an optimized matrix module. The matrix technology reaches higher module efficiency (19.3% compared to 18.6% with a half-cell module). However, more silicon is used per module. This shows that – simply speaking – shingle matrix technology does not get the best out of the host wafer but out of the module area. Therefore, shingle matrix module technology is an attractive alternative to wire soldering with half-cut cells for BIBV as well as for standard modules.

Seven matrix modules were built on a glass area of 1700 × 1000 mm^2. They feature a power up to 322 W_p and an efficiency of up to 18.8%. In experiment as well as in a detailed shingle-cell-to-module simulation, a relative power loss of −4.5% is obtained. The most important points in order to build highly efficient matrix modules, namely low glass margins, low damage cut shingles and small shingle overlap are presently under development at Fraunhofer ISE.

Long-term stability for modules with similar material was already shown for linear shingled modules by Fraunhofer ISE [17]. A batch of 10 modules is currently under test to show the same for matrix interconnected shingles. The test sequences according to IEC 61215 [23] includes TC200, humidity freeze, DH1000, mechanical load and hot-spot endurance.

Matrix integrated into a MorphoColor® façade element was presented which shows the aesthetic attractiveness of such modules. Technology wise matrix shingling offers a solution for upscaling flexible BIPV productions with a very high design flexibility.

ACKNOWLEDGEMENT

This work was funded from the Federal Ministry of Economic Affairs and Climate Action (BMWK) under the contract number 03EE1026A with the acronym Shirkan.

5 REFERENCES

[1] P.R. Shukla, J. Skea, R. Slade, A. Al Khourdajie, R. van Diemen, D. McCollum, M. Pathak, S. Some, P. Vyas, R. Fradera, M. Belkacemi, A. Hasija, G. Lisboa, S. Luz, J. Malley, (eds.), “IPCC, 2022: Summary for Policymakers. In: Climate Change 2022: Mitigation of Climate Change. Contribution of Working Group III to the Sixth Assessment Report of the Intergovernmental Panel on Climate Change,” 2022.

[2] Jr Donald C Dickson, “Photo-voltaic semiconductor apparatus or the like,” May 31, 1960.

[3] *Solaria: Solar Panels for Home & Business*. company homepage. [Online]. Available: https://www.solaria.com/solar-panels (accessed: Aug. 18 2022).

[4] *SunPower Performance Solar Panels.* [Online]. Available: https://sunpower.maxeon.com/int/solar-panel-products/performance-solar-panels (accessed: Aug. 18 2022).

[5] Tongwei Solar, “Shingled monofacial module: TH635~660PMB6, 68 SC datasheet,” 2021. [Online]. Available: http://www.tw-solar.com/en/Products/PVModules/

[6] A. Mondon, N. Klasen, M. Mittag, M. Heinrich, and H. Wirth, “Comparison of Layouts for Shingled Bifacial PV Modules in Terms of Power Output, Cell-to-Module Ratio and Bifaciality,” in

Proceedings of the 35th European Photovoltaic Solar Energy Conference and Exhibition (EU PVSEC), Brussels, Belgium, 2018, pp. 1006–1010.

[7] W. Schmidt and K.-D. Rasch, "New interconnection technology for enhanced module efficiency," *IEEE Trans. Electron Devices*, vol. 37, no. 2, pp. 355–357, 1990, doi: 10.1109/16.46366.

[8] N. Klasen, D. Weißer, T. Geipel, D. H. Neuhaus, and A. Kraft, "Performance of shingled solar modules under partial shading," *Prog. Photovolt: Res. Appl.*, pp. 1–14, 2021, doi: 10.1002/pip.3486.

[9] N. Klasen, F. Lux, J. Weber, T. Roessler, and A. Kraft, "A Comprehensive Study of Module Layouts for Silicon Solar Cells Under Partial Shading," *IEEE J. Photovoltaics*, vol. 12, no. 2, pp. 546–556, 2022, doi: 10.1109/JPHOTOV.2022.3144635.

[10] B. Blasi, T. Kroyer, T. Kuhn, and O. Hohn, "The MorphoColor Concept for Colored Photovoltaic Modules," *IEEE J. Photovoltaics*, vol. 11, no. 5, pp. 1305–1311, 2021, doi: 10.1109/JPHOTOV.2021.3090158.

[11] C. Kutter *et al.*, "Decorated Building-Integrated Photovoltaic Modules: Power Loss, Color Appearance and Cost Analysis," 2018, doi: 10.4229/35THEUPVSEC20182018-6AO.8.6.

[12] P. Baliozian *et al.*, "PERC-based shingled solar cells and modules at Fraunhofer ISE," *Photovoltaics International*, vol. 43, pp. 129–145, 2019.

[13] Solarthemen Media GmbH, *Schindel-Solarmodul von ISE und M10 ist serienreif*. [Online]. Available: https://www.solarserver.de/2022/05/10/photovoltaik-stringer-zur-fertigung-von-matrix-schindelmodulen-geht-in-serie/ (accessed: Sep. 13 2022).

[14] Nils Klasen, Julian Weber, Achim Kraft, "Lateral Currents in Shingle Solar Modules Detected by Magnetic Field Imaging," *submitted to Journal of Photovoltaics*, 2022.

[15] M. Oswald, M. Turek, J. Schneider, and S. Schoenfelder, *Evaluation of Silicon Solar Cell Separation Techniques for Advanced Module Concepts*, 2013.

[16] P. Baliozian *et al.*, "Thermal Laser Separation of PERC and SHJ Solar Cells," *IEEE J. Photovoltaics*, vol. 11, no. 2, pp. 259–267, 2021, doi: 10.1109/JPHOTOV.2020.3041251.

[17] T. Rößler *et al.*, "Progress in shingle interconnection based on electrically conductive adhesives at Fraunhofer ISE," *Aip Conf Proc*, 2022.

[18] P. Baliozian *et al.*, "Postmetallization "Passivated Edge Technology" for Separated Silicon Solar Cells," *IEEE J. Photovoltaics*, vol. 10, no. 2, pp. 390–397, 2020, doi: 10.1109/JPHOTOV.2019.2959946.

[19] M. Mittag and M. Ebert, "Systematic PV module optimization with the cell-to-module (CTM) analysis software," *Photovoltaics International*, no. 36, pp. 97–104, 2017.

[20] M. Mittag, T. Zech, M. Wiese, D. Blaesi, M. Ebert, and H. Wirth, "Cell-to-Module (CTM) analysis for photovoltaic modules with shingled solar cells," in *44th IEEE PV Specialist Conference PVSC*.

[21] J. Schneider, H. Hanifi, D. Daßler, M. Pander, F. Kaule, and M. Turek, "Half-cell solar modules: The new standard in PV production?," *Photovoltaics International*, vol. 2019.

[22] M. Devoto Acevedo, T. Timofte, A. Halm, and D. Tune, *Improved Measurement of the Contact Resistivity of ECA-Based Joints*, 2021.

[23] *IEC 61215-2 Terrestrial photovoltaic (PV) modules – Design qualification and type approval – Part 2: Test procedures*, 2016.

6 ANNEX

SmartCalc.Module half-cell simulation

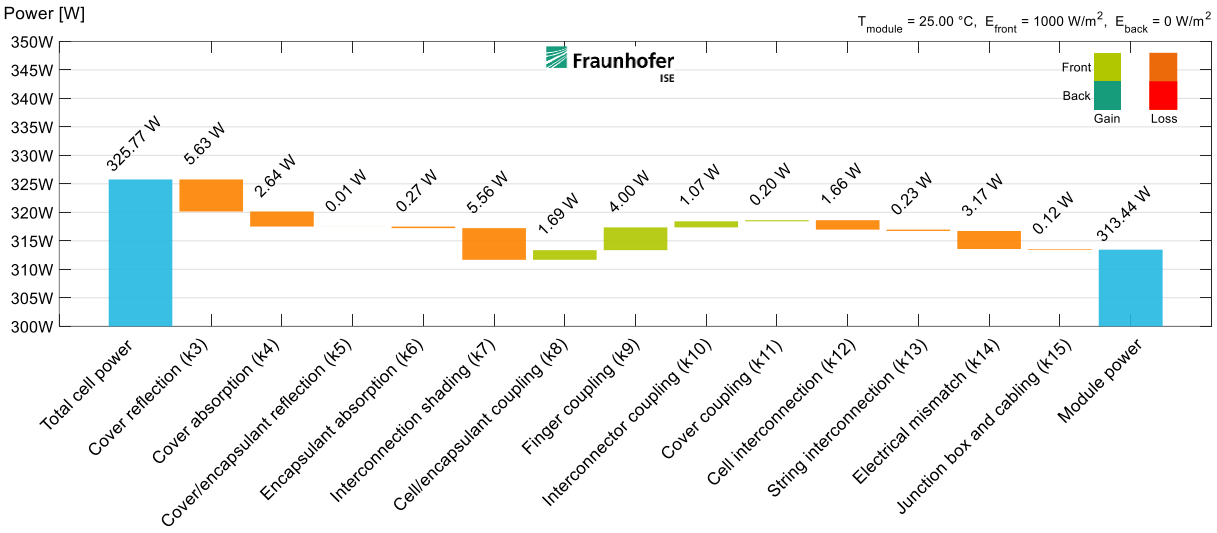

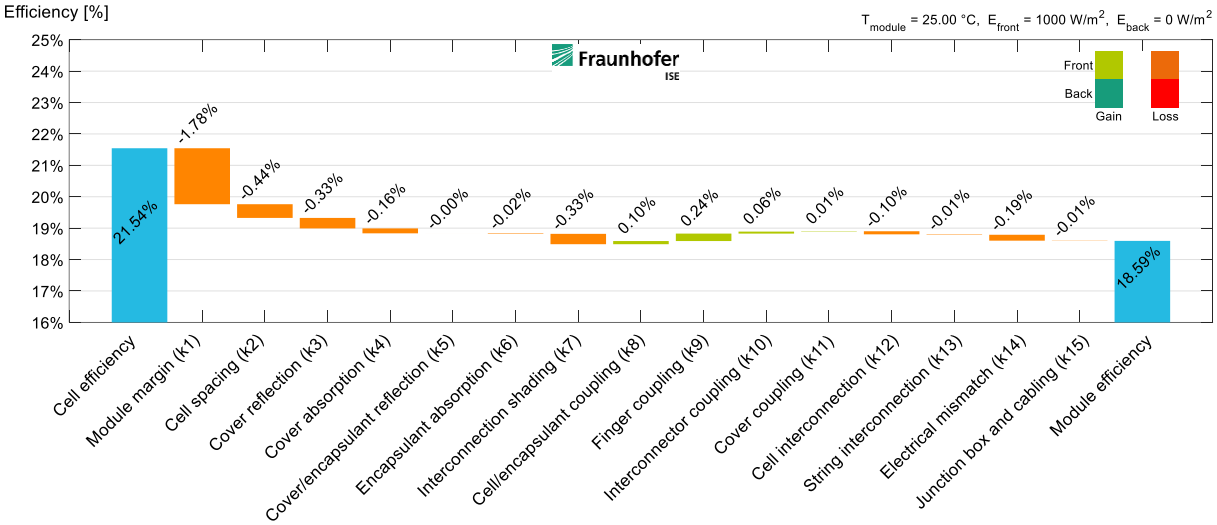

SmartCalc.Module matrix simulation: Scenario 1

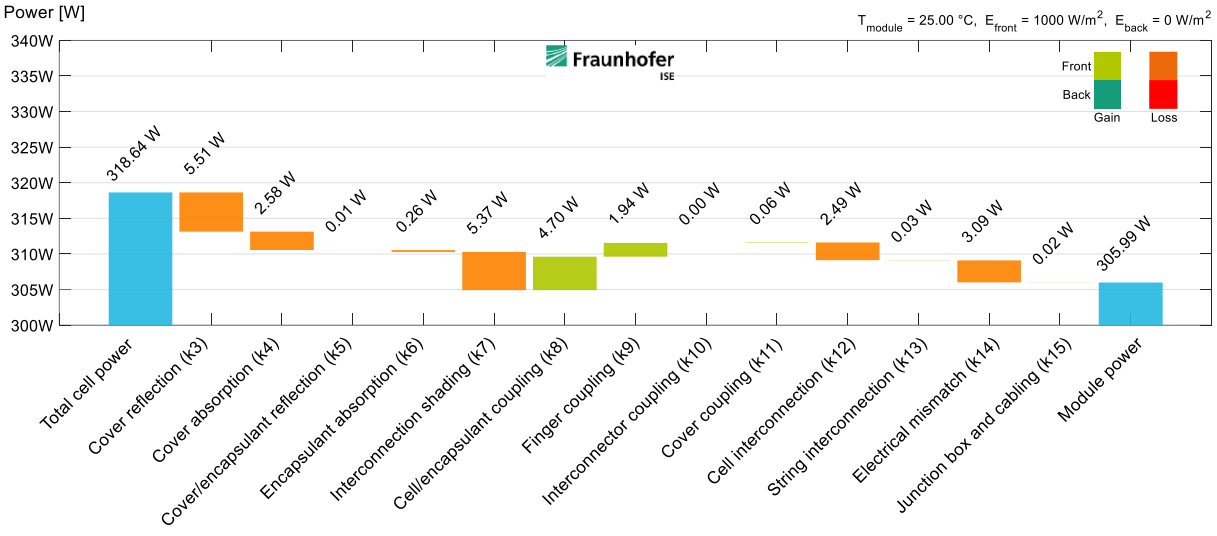

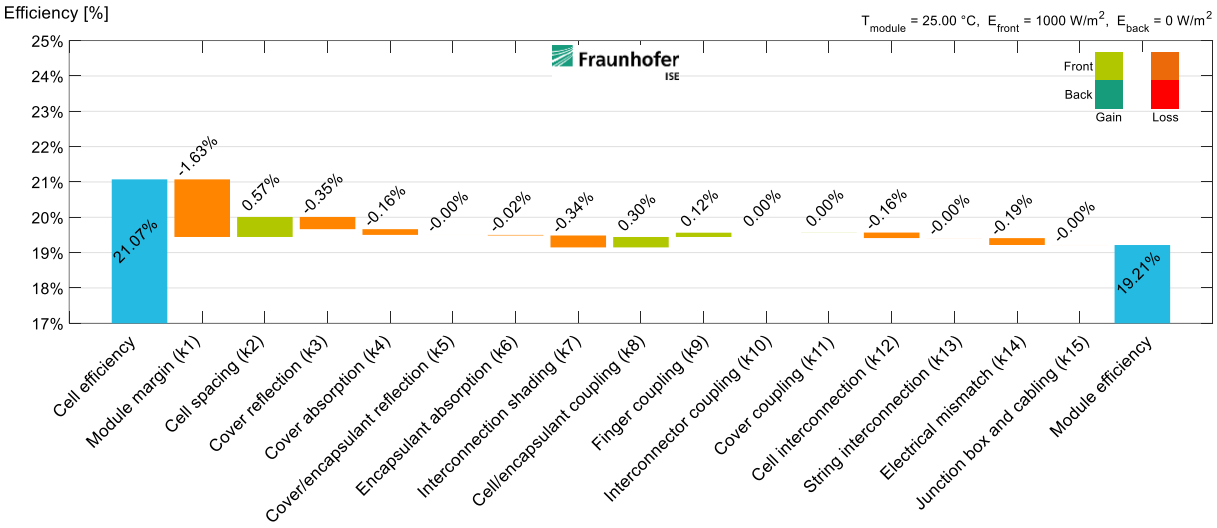

SmartCalc.Module matrix simulation: Scenario 2